Search in the Two-Photon Final State for Evidence of New Particle Production at the Large Hadron Collider

Rachel P. Yohay
University of Virginia
rpy3y@virginia.edu

December 6, 2011

Contents

Chapter 1

Introduction

Chapter 2

Overview of the Standard Model of Particle Physics

I call it...the Aristocrats.

In the 1960s, Sheldon Glashow, Steven Weinberg, and Abdus Salam proposed a mathematical framework that unified the electromagnetic and weak forces at an energy scale in the hundreds of GeV/c, as well as a mechanism for breaking the electroweak symmetry at low energies [1]. At the same time, Murray Gell-Mann introduced the concept of quarks to describe hadron spectroscopy, a concept that would later grow into quantum chromodynamics (QCD), the full theory of the strong force [2]. These two key developments motivated the unified representation of particle physics as a set of fields whose dynamics are invariant under the Standard Model gauge group

$$SU(3)_C \bigotimes SU(2)_L \bigotimes U(1)_{EM} \tag{2.1}$$

where $SU(3)_C$ describes the quark QCD interactions, $SU(2)_L$ describes the weak interactions among quarks and leptons, and $U(1)_{EM}$ describes the electromagnetic interaction.

The Standard Model, in particular the electroweak theory, has been an extremely successful predictor of particle production and interaction cross-sections and decay rates, as well as of the exact masses of the electroweak force carriers. The case for the validity of the Standard Model was bolstered by the many precision QCD and electroweak measurements carried out at the Large Electron-Positron (LEP) collider, which ran from 1989-2000 at center-of-mass energies between 65 and 104 GeV/c [3]. Figure 1 shows some of the highlights of the LEP program.

However, there are still deep theoretical problems with the Standard Model, stemming from the introduction of the Higgs scalar into the theory to break electroweak symmetry [4]. Since the Higgs self-energy diagram is quadratically sensitive to the ultraviolet cutoff scale(footnote: this is a general property of scalar fields), and assuming that there are no new important energy scales of physics between the weak scale ($\mathcal{O}(10^2$ GeV/c)) and the Planck scale ($\mathcal{O}(10^{19}$ GeV/c)), in order to be consistent with experimental measurements, this diagram must include a remarkable 17-orders-

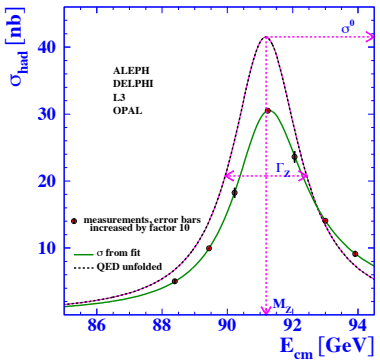

(a) Total hadronic cross-section as a function of collider center-of-mass energy.

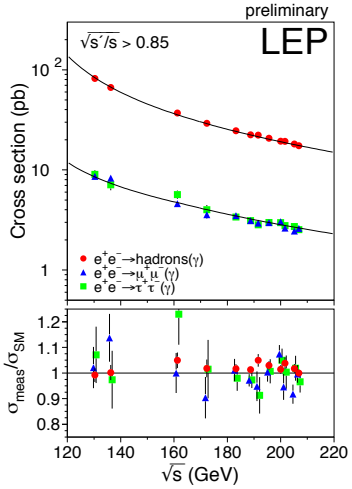

(b) Measured and predicted dependence of the $q\bar{q}$, $\mu^+\mu^-$, and $\tau^+\tau^-$ pair production cross sections on LEP center-of-mass energy.

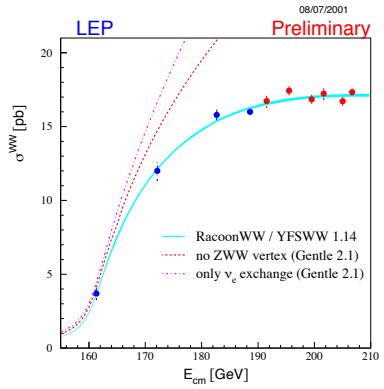

(c) Measured and predicted dependence of the W^+W^- pair production cross section on LEP center-of-mass energy.

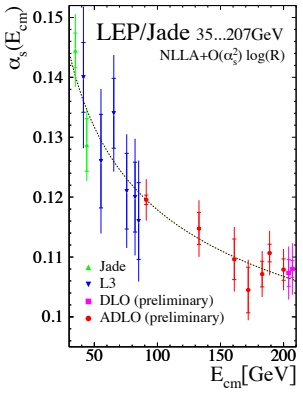

(d) Measured and predicted dependence of the strong coupling constant α_s on LEP center-of-mass energy.

Figure 2.1: Selected LEP measurements demonstrating its contribution to the precise understanding of the Standard Model. Reprinted from [3].

of-magnitude cancellation that is otherwise poorly motivated [5]. The quest to find new physics at an intermediate energy scale between the weak and Planck scales, and thus extend the Standard Model, was the driving force behind the construction of the Large Hadron Collider (LHC) in 2009, the world's highest energy particle accelerator to date.

In this chapter I will briefly describe the Standard Model particle content, the theory and major results of electroweak symmetry breaking (EWSB), and the problems that the Standard Model is as yet ill-prepared to address.

2.1 Particle Content

2.2 Electroweak Symmetry Breaking and the Higgs Mechanism

2.3 The Hierarchy Problem, The Origins of Mass, and Fine Tuning

Chapter 3

The Supersymmetric Extension to the Standard Model

3.1 SUSY Lagrangian and Particle Content, SUSY Breaking

3.2 Dark Matter and the WIMP Miracle

3.3 Gauge-Mediated SUSY Breaking

3.4 Experimental Status of SUSY

Collider searches for evidence of supersymmetry began in earnest in the 1980s ([6]) and continue to this day. Most recently, the LHC and Tevatron[1] experiments have set the strictest limits on a variety of SUSY breaking scenarios, including GMSB and mSUGRA (discussed below).

Figure X shows the current limits set by the CMS experiment on the mSUGRA model (with $\tan\beta = 10$) in the m_0-$m_{1/2}$ plane. (Note that although the plot is truncated at $m_0 = 1000$ GeV/c^2, some searches are sensitive out to $m_0 \sim 2000$ GeV/c^2.) Although the LHC has pushed m_0 above $\sim$1 TeV/c^2 for $m_{1/2}$ up to $\sim$400 GeV/c^2, casting some doubt onto the theory's prospects for solving the hierarchy problem, there is still a sizable chunk of mSUGRA parameter space that is not ruled out by collider experiments. Furthermore, parts of the CMS unexplored regions overlap with areas allowed by astrophysics experiments [8].

Figure X shows the most up-to-date limit (using 1 fb^{-1} of integrated luminosity collected by the ATLAS experiment [10] at the LHC) on the Snowmass Points and Slopes (SPS) model of minimal GMSB (mGMSB), dubbed SPS8 [11]. SPS8 represents the simplest class of GMSB models described in Sec. X. The best limits on a variety of general gauge mediation (GGM) models, from the same ATLAS study, are shown

[1] Located on the Fermilab site in Batavia, Illinois, the Tevatron was a proton-antiproton collider operating at 1.96 TeV center-of-mass energy. The Tevatron ran from 1987 to 2011 [7].

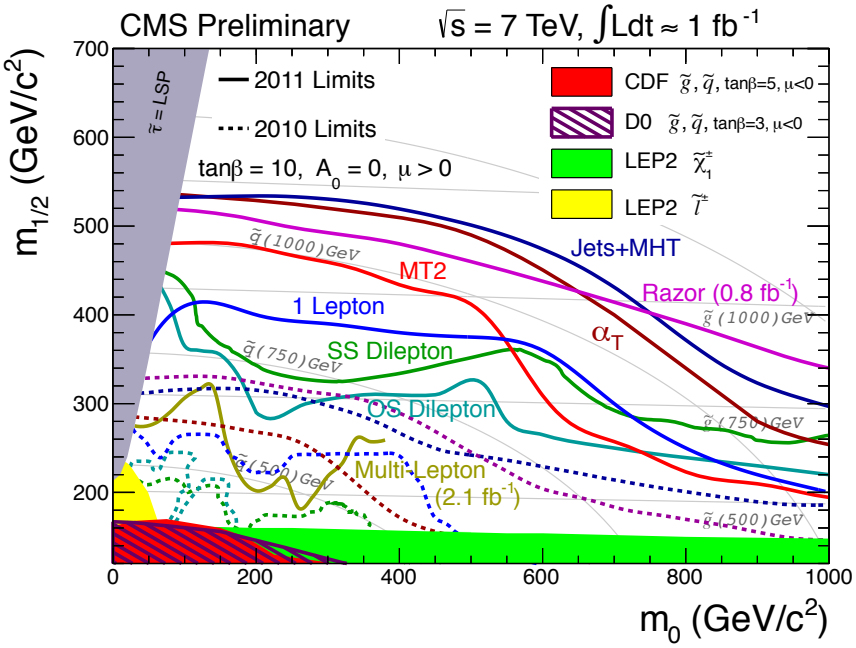

Figure 3.1: CMS limits on mSUGRA with tan $\beta = 10$. The limits set by individual searches are shown as separate colored lines. Solid lines refer to 2011 searches (i.e. using an integrated luminosity of $\sim$1 fb^{-1}), while dashed lines refer to 2010 searches ($\sim$36 pb^{-1}). Reprinted from [9].

in Figure X. In these models, no assumptions are made about the specific parameters common to many gauge mediation models (e.g. the number of messengers or the relationship between the messenger mass and the SUSY breaking scale). Instead, it is only assumed that the lightest neutralino is light enough to be produced on-shell at the LHC (by setting M_1 and M_2 appropriately, see Sec. X) and that it decays to a gravitino, that the gravitino is extremely relativistic (mass of order eV-keV), and that the gravitino is stable. The one-dimensional scan over SUSY breaking scales in the SPS8 model (in which the full sparticle spectrum is specified by the model parameters) is replaced by a two-dimensional scan over gluino and lightest neutralino mass in the GGM models (in which all sparticles except the gluino, first- and second-generation squarks, and neutralinos are forced to be at $\sim$1.5 TeV/c^2, effectively decoupling them from the dynamics that can be probed with 1 fb^{-1} at a 7 TeV/c pp collider).

In general, the lifetime of the lightest neutralino in GMSB models can take on any value between hundreds of nanometers to a few kilometers depending on the mass of the lightest neutralino and the SUSY breaking scale [13]. The search published in [12] (from which Figs. X and X are culled) considers only *prompt* neutralino variants, i.e. with neutralino lifetime short enough that the distance traveled by the neutralino before decay cannot be resolved by the detector. The most recent limits on non-prompt neutralino models were set by the Collider Detector at Fermilab (CDF) collaboration with X fb^{-1}, and are shown in Figure X.

Table X summarizes the current best limits on the GMSB scenarios discussed in this section.

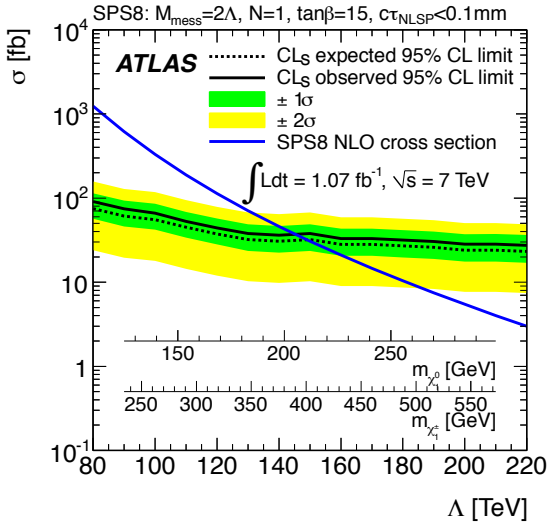

Figure 3.2: ATLAS cross section upper limit on the SPS8 [11] model of mGMSB as a function of SUSY breaking scale Λ, lightest neutralino mass $m_{\tilde{\chi}_1^0}$, or lightest chargino mass $m_{\tilde{\chi}_1^\pm}$. Values of Λ, $m_{\tilde{\chi}_1^0}$, or $m_{\tilde{\chi}_1^\pm}$ below the intersection point between the blue (predicted SPS8 cross section) and black (observed cross section upper limit) curves are excluded. The model parameters listed above the plot are defined in Sec. X. Reprinted from [12].

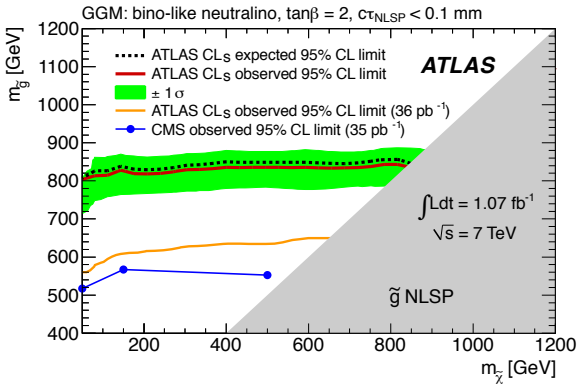

Figure 3.3: ATLAS exclusion contour in the $m_{\tilde{g}}$-$m_{\tilde{\chi}}$ plane. Values of $m_{\tilde{g}}$-$m_{\tilde{\chi}}$ below the red curve are excluded. The gray region is theoretically excluded in the GGM models considered. "Bino-like neutralino" means that $M_2 = 1.5$ TeV/c^2. Reprinted from [12].

Chapter 4

The Large Hadron Collider

Chapter 5

The Compact Muon Solenoid Experiment

5.1 The Detectors and Their Operating Principles

5.1.1 Tracking System

Pixel Detector

Silicon Strip Tracker

5.1.2 Electromagnetic Calorimeter

5.1.3 Hadronic Calorimeter

5.1.4 Muon System

5.1.5 Far Forward Calorimetry

5.2 Triggering, Data Acquisition, and Data Transfer

5.2.1 Level 1 and High Level Trigger Systems

5.2.2 Data Acquisition System

5.2.3 Data Processing and Transfer to Computing Centers

Chapter 6

Event Selection

6.1 HLT

6.2 Object Reconstruction

6.2.1 Photons

6.2.2 Electrons

6.2.3 Jets and Missing Transverse Energy

6.3 Photon Identification Efficiency

Chapter 7

Data Analysis

7.1 Modeling the QCD Background

7.1.1 Systematic Errors

7.1.2 Jet Energy Scale Uncertainty

The dijet p_T reweighting method utilizes jets corrected for imperfect calorimeter response (see Sec. X for a description of the jet reconstruction and correction procedure). Since the applied jet energy scale (JES) factor has an error associated to it due to the limitations of the JES derivation ([14] and Sec. X), this uncertainty must be propagated to the uncertainty on the dijet p_T weights.

The JES contribution to the dijet p_T weights is estimated by performing 1000 pseudo-experiments on each of the $\gamma\gamma$ and ff samples. For the purpose of estimating the JES error, the results of the true experiment may be thought of as a set of measurements:

- The set of **uncorrected jet 4-vectors** corresponding to the **leading EM object** in the $\boldsymbol{\gamma\gamma}$ sample $\left\{ p_{j1}^{\mu 1}, p_{j1}^{\mu 2}, ..., p_{j1}^{\mu N_{\gamma\gamma}} \right\}$
- The set of **uncorrected jet 4-vectors** corresponding to the **trailing EM object** in the $\boldsymbol{\gamma\gamma}$ sample $\left\{ p_{j2}^{\mu 1}, p_{j2}^{\mu 2}, ..., p_{j2}^{\mu N_{\gamma\gamma}} \right\}$
- The set of **JES** accompanying the uncorrected jet 4-vectors corresponding to the **leading EM object** in the $\boldsymbol{\gamma\gamma}$ sample $\left\{ c_{j1}^{1}, c_{j1}^{2}, ..., c_{j1}^{N_{\gamma\gamma}} \right\}$
- The set of **JES** accompanying the uncorrected jet 4-vectors corresponding to the **trailing EM object** in the $\boldsymbol{\gamma\gamma}$ sample $\left\{ c_{j2}^{1}, c_{j2}^{2}, ..., c_{j2}^{N_{\gamma\gamma}} \right\}$
- The set of **JES uncertainties** accompanying the uncorrected jet 4-vectors corresponding to the **leading EM object** in the $\boldsymbol{\gamma\gamma}$ sample $\left\{ \sigma_{cj1}^{1}, \sigma_{cj1}^{2}, ..., \sigma_{cj1}^{N_{\gamma\gamma}} \right\}$

- The set of **JES uncertainties** accompanying the uncorrected jet 4-vectors corresponding to the **trailing EM object** in the $\gamma\gamma$ sample $\left\{\boldsymbol{\sigma}^{\mathbf{1}}_{\mathrm{cj_2}}, \boldsymbol{\sigma}^{\mathbf{2}}_{\mathrm{cj_2}}, ..., \boldsymbol{\sigma}^{\mathrm{N}_{\gamma\gamma}}_{\mathrm{cj_2}}\right\}$
- The set of **uncorrected jet 4-vectors** corresponding to the **leading EM object** in the ff sample $\left\{\mathrm{p}^{\boldsymbol{\mu 1}}_{\mathrm{j_1}}, \mathrm{p}^{\boldsymbol{\mu 2}}_{\mathrm{j_1}}, ..., \mathrm{p}^{\mu \mathrm{N}_{\mathrm{ff}}}_{\mathrm{j_1}}\right\}$
- The set of **uncorrected jet 4-vectors** corresponding to the **trailing EM object** in the ff sample $\left\{\mathrm{p}^{\boldsymbol{\mu 1}}_{\mathrm{j_2}}, \mathrm{p}^{\boldsymbol{\mu 2}}_{\mathrm{j_2}}, ..., \mathrm{p}^{\mu \mathrm{N}_{\mathrm{ff}}}_{\mathrm{j_2}}\right\}$
- The set of **JES** accompanying the uncorrected jet 4-vectors corresponding to the **leading EM object** in the ff sample $\left\{\mathrm{c}^{\mathbf{1}}_{\mathrm{j_1}}, \mathrm{c}^{\mathbf{2}}_{\mathrm{j_1}}, ..., \mathrm{c}^{\mathrm{N}_{\mathrm{ff}}}_{\mathrm{j_1}}\right\}$
- The set of **JES** accompanying the uncorrected jet 4-vectors corresponding to the **trailing EM object** in the ff sample $\left\{\mathrm{c}^{\mathbf{1}}_{\mathrm{j_2}}, \mathrm{c}^{\mathbf{2}}_{\mathrm{j_2}}, ..., \mathrm{c}^{\mathrm{N}_{\mathrm{ff}}}_{\mathrm{j_2}}\right\}$
- The set of **JES uncertainties** accompanying the uncorrected jet 4-vectors corresponding to the **leading EM object** in the ff sample $\left\{\boldsymbol{\sigma}^{\mathbf{1}}_{\mathrm{cj_1}}, \boldsymbol{\sigma}^{\mathbf{2}}_{\mathrm{cj_1}}, ..., \boldsymbol{\sigma}^{\mathrm{N}_{\mathrm{ff}}}_{\mathrm{cj_1}}\right\}$
- The set of **JES uncertainties** accompanying the uncorrected jet 4-vectors corresponding to the **trailing EM object** in the ff sample $\left\{\boldsymbol{\sigma}^{\mathbf{1}}_{\mathrm{cj_2}}, \boldsymbol{\sigma}^{\mathbf{2}}_{\mathrm{cj_2}}, ..., \boldsymbol{\sigma}^{\mathrm{N}_{\mathrm{ff}}}_{\mathrm{cj_2}}\right\}$

Each pseudo-experiment is identical to the true experiment in all respects except for the EM-matched jet p^{μ}, i.e. all EM object 4-vectors remain the same, as do the 4-vectors of non-EM-matched jets, and the sizes of the $\gamma\gamma$ and ff samples remain the same.[1] In each pseudo-experiment, a random corrected EM-matched jet p^{μ} is generated according to the uncertainty

If jet energy fluctuates below 20 GeV, there could be a slight effect due to not finding the matched jet. We have checked in data that the number of times a jet is not found due to ET threshold is only n in large m. Furthermore, the low ET cut is at 25 GeV, meaning the JEC would have to be mismeasured by at least 20 percent. Since the typical JEC uncertainty is no more than 5 percent, a mismeasurement of this type is represents a 4sigma event, and should occur in 0.1 percent of cases. Need to check that this is insignificant.

7.2 Modeling the Electroweak Background

7.3 Results

[1] The $\mathrm{E}_{\mathrm{T}}^{\mathrm{miss}}$ is uncorrected and therefore unaffected by a change in the JES.

Chapter 8

Interpretation of Results in Terms of GMSB Models

8.1 Simplified Models

8.2 Upper Limit Calculation

8.3 Cross Section Upper Limits

8.4 Exclusion Contours

Chapter 9

Conclusion

Bibliography

[1] S.L. Glashow, J. Iliopoulis, and L. Maiani, *Phys. Rev. D* **2** (1970) 1285; S.L. Glashow, *Nucl. Phys.* **22(4)** (1961) 579; J. Goldstone, A. Salam, and S. Weinberg, *Phys. Rev.* **127** (1962) 965; S. Weinberg, *Phys. Rev. Lett.* **19** (1967) 1264; A. Salam and J.C. Ward, *Phys. Lett.* **13(2)** (1964) 168.

[2] M. Gell-Mann, *Phys. Lett.* **8** (1964) 214; G. Zweig, *CERN* **8419/TH. 412** (1964) (unpublished).

[3] J. Drees, *Int. J. Mod. Phys.* **A17** (2002) 3259.

[4] P.W. Higgs, *Phys. Lett.* **12(2)** (1964) 132; P.W. Higgs, *Phys. Rev. Lett.* **13** (1964) 508; P.W. Higgs, *Phys. Rev.* **145** (1966) 1156.

[5] I. Aitchison, *Supersymmetry in Particle Physics: An Elementary Introduction* (Cambridge University Press, Cambridge 2007), p. 4.

[6] E. Fernandez et al., *Phys. Rev. Lett.* **54** (1985) 1118; E. Fernandex et al., *Phys. Rev.* **D35** (1987) 374; D. Decamp et al., *Phys. Lett.* **B237(2)** (1990) 291; F. Abe et al., *Phys. Rev. Lett.* **75** (1995) 613; S. Abachi et al., *Phys. Rev. Lett.* **75** (1995) 618; G. Alexander et al., *Phys. Lett.* **B377(4)** (1996) 273; S. Aid et al., *Z. Phys.* **C71(2)** (1996) 211; S. Aid et al., *Phys. Lett.* **B380(3-4** (1996) 461; B. Aubert et al., *Phys. Rev. Lett.* **95** (2005) 041802.

[7] `http://en.wikipedia.org/wiki/Tevatron`.

[8] O. Buchmueller et al., *CERN-PH-TH/2011-220* (2011).

[9] `https://twiki.cern.ch/twiki/bin/view/CMSPublic/PhysicsResultsSUS`.

[10] G. Aad et al., *JINST* **3** (2008) S08003.

[11] B.C. Allanach et al., *Eur. Phys. J.* **C25** (2002) 113.

[12] G. Aad et al., *CERN-PH-EP-2011-160* (2011).

[13] S. P. Martin, *A Supersymmetry Primer* **v4** (2006) 86. arXiv:hep-ph/9709356.

[14] S. Chatrchyan et al., *JINST* **6** (2011) P11002.